Baltic Astronomy, vol. 17, 1–19, 2008

YOUNG STARS IN THE CAMELOPARDALIS DUST AND MOLECULAR CLOUDS. III. THE GL 490 REGION

V. Straižys and V. Laugalys

Institute of Theoretical Physics and Astronomy, Vilnius University, Goštauto 12, Vilnius LT-01108, Lithuania

Received 2007 November 2; accepted 2007 November 30

Abstract. Using the infrared photometry data extracted from the 2MASS, IRAS and MSX databases, 50 suspected young stellar objects (YSOs) are selected from about 37 500 infrared objects in the $3° \times 3°$ area with the center at ℓ, b = 142.5°, +1.0°, in the vicinity of the young stellar object GL 490 in the dark cloud DoH 942 (Dobashi et al. 2005). The spectral energy distributions between 700 nm and 100 μm suggest that most of the selected objects may be YSOs of classes I and II. In the color-magnitude diagram K_s vs. $H{-}K_s$ the suspected YSOs occupy an area right of the main sequence what can be interpreted as being caused by the effects of luminosity, interstellar and circumstellar reddening and infrared thermal emission in circumstellar envelopes and disks.

Key words: stars: formation – stars: pre-main-sequence – infrared: stars – ISM: dust, extinction, clouds – Galaxy: open clusters and associations: individual (Cam OB1)

1. INTRODUCTION

In the previous papers (Straižys & Laugalys 2007a,b, Papers I and II) we made census of young stellar objects in the Camelopardalis segment of the Local spiral arm (ℓ, b = 132–158°, ±12°). More than 40 stars of the Cam OB1 association, about 20 young stars of lower masses exhibiting emission in Hα or belonging to irregular variable stars of types IN and IS, as well as 42 infrared young stellar objects (YSOs) in the Local arm were identified. Among the latter objects, the most prominent is a high-mass young object GL 490, embedded in the densest part of the dust cloud DoH 942 (Dobashi et al. 2005). [1] All of the identified YSOs have $H{-}K_s \geq 1.0$, since bluer objects were difficult to identify among thousands of objects having no relation to star forming.

Trying to find more YSOs in the area, we reduced the limiting $H{-}K_s$ from 1.0 to 0.75, decreasing at the same time the size of the investigated area down to $3° \times 3°$. In the area centered at ℓ, b = 142.5°, +1.0° we have analyzed the infrared objects measured in the 2MASS, IRAS and MSX surveys. For IRAS objects the

[1] The clouds in the Dobashi et al. (2005) high-resolution atlas in Paper I were named Tokyo clouds.

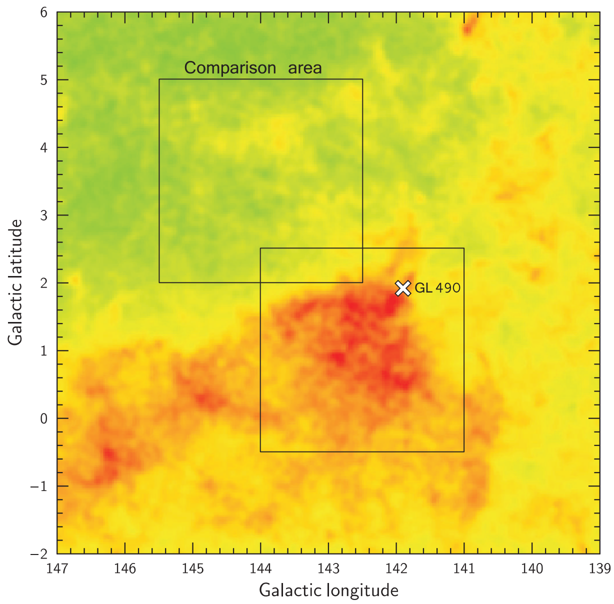

Fig. 1. Positions of the GL 490 area and the comparison area in Galactic coordinates. In the background dust clouds from the Dobashi et al. (2005) atlas are shown. The position of YSO GL 490 in the corner of the DoH 942 cloud is shown as the white cross.

selection limit of H–K_s was decreased from 0.75 to 0.5.

For a comparison, the infrared objects were also considered in the standard area of the same size centered at ℓ, b = 144.0°, +3.5°, in a relatively transparent direction. Both areas are shown in Figure 1, with dust clouds from the Dobashi et al. (2005) atlas shown in the background.

2. IDENTIFICATION OF THE PRE-MAIN-SEQUENCE OBJECTS

Figure 2 shows the J–H vs. H–K_s diagram for about 37 500 stars measured in the 2MASS survey with the errors $\leq$ 0.05 mag (Cutri et al. 2003; Skrutskie et al. 2006). The picture is quite similar to that shown in Fig. 1 of Paper II. In the comet-like crowding of dots the orange line designates the intrinsic main sequence, the yellow line K–M giants and the blue line the intrinsic locus of T Tauri-type stars from Meyer et al. (1997). In both figures the 'comet head' is composed mostly of normal stars of different spectral classes with small interstellar extinction. The upper 'tail' is composed of normal heavily reddened background stars, mostly of K and M giants.

As it was shown in Paper II, the lower 'tail', running more or less along the black-body line, contains YSOs of different masses and evolutionary stages. In this part of the diagram, along with the young objects, we expect to find also M-type giants of the latest subclasses, including oxygen-rich and carbon-rich long-period variables, OH/IR stars, carbon-rich stars of spectral type N, Be stars, infrared dusty galaxies and quasars. Since JHK photometry is not sufficient for the identification of young stars, either spectroscopic or infrared photometric observations at longer wavelengths are essential.

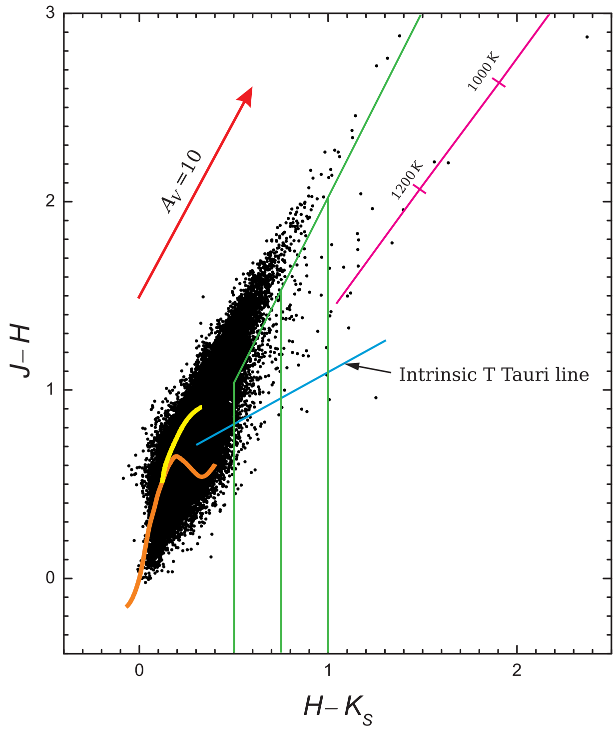

Fig. 2. The J–H vs. H–K_s diagram for 37 500 objects in the GL 490 area. The intrinsic main-sequence and K–M giant lines are shown in orange and yellow, respectively. The blue line designates the intrinsic locus of T Tauri stars, the violet line is the locus of black bodies. The length of the reddening vector (shown in red) corresponds to the extinction in the V passband of 10 mag. The three green vertical lines and the reddening line running through the point J–H = H–K_s = 0 isolate the regions where the presence of young stellar objects was investigated (see the text).

Suspected YSOs in Figure 2 were isolated in the box limited by the three lines: from the left and right sides by two vertical lines at H–K_s = 0.75 and 1.0, and from the top by the interstellar reddening line corresponding to

$$Q_{JHK} = (J - H) - 1.85(H - K_s) = 0.0.$$

As was shown in Paper II this condition excludes the majority of normal stars of various temperatures, luminosities and reddenings (except heavily reddened O–B stars and the coolest M giants and dwarfs). The objects with H–$K_s \geq 1.0$ were considered in Paper II. In the box between H–K_s = 0.75 and 1.0 we found 37 objects.

Apart from YSOs, in this part of the diagram we expect to find reddened M-type giants of the latest subclasses, AGB OH/IR stars, carbon-rich stars of spectral type N, Be stars, dusty spiral galaxies and quasars. In our sample of 37 objects we identified, using the Simbad database, two carbon stars, one galaxy and two radio sources. The remaining 32 objects are listed in Table 1, continuing the same sequential numeration as in Table 1 of Paper II. As earlier, magnitudes, color indices and Q-parameters are rounded to two decimal places. Seven objects

Table 1. Suspected YSOs with H–K_s between 0.5 and 1.0 in the $3° \times 3°$ area centered at ℓ, $b = 142.5°$, $+1.0°$.

SL	ℓ	b	F	J	H	K_s	J–H	H–K_s	Q_{JHK}	IRAS, MSX
Objects with H–K_s between 0.75 and 1.00										
143	141.859	1.753	–	15.58	14.21	13.42	1.37	0.79	–0.09	
144	141.900	1.666	16.30	12.55	11.34	10.46	1.20	0.88	–0.42	
145	141.938	1.764	–	15.24	13.73	12.84	1.51	0.90	–0.14	
146	141.955	1.740	18.79	13.88	12.49	11.69	1.39	0.80	–0.10	
147	141.967	1.715	–	14.68	13.08	12.20	1.60	0.88	–0.03	
148	142.006	1.749	19.16	14.56	13.19	12.38	1.37	0.81	–0.13	
149*	142.041	1.849	–	15.41	13.91	13.09	1.50	0.82	–0.01	
150	142.164	1.670	–	15.30	13.77	12.94	1.53	0.84	–0.02	
151	142.243	1.740	–	15.16	13.74	12.95	1.42	0.79	–0.04	
152	142.265	1.693	–	15.02	13.63	12.80	1.39	0.82	–0.13	
153	142.299	0.619	16.51	11.98	10.99	10.23	1.00	0.76	–0.42	
154	142.341	1.592	19.38	14.34	12.96	12.20	1.37	0.77	–0.05	
155	142.403	1.220	18.56	14.76	13.58	12.83	1.18	0.75	–0.20	
156	142.477	1.683	–	15.48	13.98	13.02	1.50	0.96	–0.27	
157	142.529	1.577	–	15.52	13.97	13.12	1.56	0.85	–0.01	
158	142.580	1.539	14.63	11.59	10.37	9.38	1.22	0.98	–0.60	03261+5803, MSX
159	142.633	1.418	18.10	14.06	12.81	12.02	1.26	0.79	–0.20	03260+5755
160	142.647	1.185	20.35	15.25	14.05	13.25	1.20	0.80	–0.29	
161	142.680	1.425	18.13	14.17	12.92	12.12	1.25	0.81	–0.24	03260+5755
162*	142.700	1.689	17.78	13.17	11.86	10.92	1.31	0.94	–0.43	
163	142.743	1.946	17.51	13.89	12.81	11.82	1.08	0.99	–0.75	03289+5818
164*	142.746	1.390	20.27	15.56	14.04	13.19	1.53	0.84	–0.03	
165*	142.972	1.878	15.40	12.16	10.99	10.10	1.18	0.89	–0.47	MSX
166	142.981	1.707	19.79	15.45	14.26	13.43	1.19	0.83	–0.35	
167*	142.990	1.751	18.61	14.32	12.95	12.18	1.38	0.77	–0.05	
168*	142.993	1.755	18.66	13.82	12.45	11.59	1.38	0.86	–0.21	
169	143.004	1.753	18.72	14.60	13.16	12.37	1.44	0.79	–0.02	03298+5758
170	143.008	1.429	18.84	15.15	13.93	13.17	1.22	0.76	–0.19	

Table 1. Continued

SL	ℓ	b	F	J	H	K_s	J–H	H–K_s	Q_{JHK}	IRAS, MSX
171	143.224	0.941	16.60	10.03	8.33	7.37	1.70	0.96	–0.08	MSX
172	143.369	1.262	18.62	14.75	13.64	12.86	1.11	0.78	–0.32	
173	143.908	0.644	13.63	11.78	10.89	10.03	0.89	0.85	–0.69	03304+5633
174*	143.958	–0.458	19.65	15.34	14.21	13.37	1.13	0.84	–0.42	03262+5536
Objects with H–K_s between 0.50 and 0.75										
175*	141.245	1.375	13.43	11.72	11.23	10.70	0.49	0.53	–0.50	03167+5840
176*	141.353	0.351	14.49	12.40	11.66	11.04	0.73	0.62	–0.42	03135+5743
177	141.927	2.004	16.38	13.16	12.13	11.44	1.02	0.70	–0.27	03239+5849
178	141.988	0.964	19.91	14.70	13.65	13.02	1.06	0.63	–0.10	03199+5755
179	142.005	0.839	–	15.38	14.46	13.85	0.93	0.60	–0.18	03194+5746
180	142.075	1.163	15.06	12.05	11.19	10.45	0.86	0.73	–0.49	03213+5801
181*	142.457	1.722	19.77	15.22	14.32	13.71	0.90	0.60	–0.21	03263+5816
182	142.553	0.847	20.35	15.30	14.31	13.68	0.98	0.63	–0.18	03231+5730
183*	142.604	1.201	14.02	12.36	11.81	11.22	0.56	0.59	–0.53	03248+5745
184	142.650	1.428	17.28	13.02	11.80	11.11	1.23	0.69	–0.05	03260+5755
185*	142.788	1.528	20.50	15.05	13.99	13.35	1.06	0.64	–0.12	03275+5755
186	142.868	1.818	18.61	14.55	13.38	12.69	1.18	0.69	–0.09	03292+5806
187	143.644	1.322	18.33	14.15	13.25	12.75	0.90	0.50	–0.02	03317+5716

Notes to Table 1:

SL 149: binary, in K brighter component at 6″;
SL 162: binary, in K fainter component at 6″;
SL 164: no object in R and very faint in K. Wrong coordinates?
SL 165: in R with tail, in K no tail;
SL 167 and 168: nearby YSOs separated by 19″;
SL 174: very faint in R and K. Wrong coordinates and IRAS identification?
SL 175, 176 and 183: probably heavily reddened Herbig Ae/Be stars (in the J–H vs. H–K_s diagram they lie well below the intrinsic T Tauri line);
SL 181: binary, in K fainter component at 10″;
SL 185: binary, in K fainter component at 12″.

Table 2. IRAS and MSX data for the suspected YSOs in the investigated area with $H–K_s \geq 0.75$. Fluxes are given in Janskys.

SL	IRAS	F_{12}	F_{25}	F_{60}	F_{100}	$F_{8.3}$	YSO type
89	03228+5834	0.24:	1.06	<4.04	<27.7	–	I
93	03233+5833	0.44	2.13	23.3	40:	–	I
95	03236+5836	90.5	290	715	1156	54.73	I
102	03290+5724	<0.26	0.17	<0.75	<44.76	–	II
107	03303+5643	<0.39	<0.25	0.69	<5.80	–	I
158	03261+5803	0.33	0.32	<3.87	<44.34	0.25	II
159	03260+5755	<0.31	0.25	<3.89	<57.19	–	II
165	–	–	–	–	–	0.14	II
169	03298+5758	0.40	0.59	6.32	26.86	–	I
171	–	–	–	–	–	0.39	II
173	03304+5633	<0.49	0.31	<0.63	<5.38	–	
174	03262+5536	<0.25	<0.25	1.15	8.35	–	I
175	03167+5840	0.75	0.34	1.51:	<26.32	–	I:
176	03135+5743	<0.57	0.20	<3.26	<25.98	–	II
177	03239+5849	<0.44	<0.36	5.93	<33.39	–	I
178	03199+5755	<0.37	<0.25	<2.01	16.05	–	I
179	03194+5746	<0.28	<0.27	0.83	<27.62	–	I
180	03213+5801	<0.29	0.34	<2.54	<33.80	–	II
181	03263+5816	<0.44	<0.26	1.29	<48.02	–	I
182	03231+5730	<0.25	<0.25	0.57:	9.12	–	I
183	03248+5745	0.31:	0.96	<2.94	<28.79	–	I
184	03260+5755	<0.31	0.25	<3.89	<57.19	–	II
185	03275+5755	<0.29	<0.31	<2.32	8.46	–	I
186	03292+5806	<0.28	0.43	<3.35	10.60	–	I
187	03317+5716	<0.30	<0.25	0.59	<33.54	–	I

of Table 1 have been measured by IRAS and three by MSX. These objects are listed in Table 2, together with five objects in the same area (SL 89, SL 93, SL 95, SL 102 and SL 107) identified in Paper II as YSOs with $H–K_s \geq 1.0$.

Additionally, in Tables 1 and 2 we list 13 objects with $H–K_s$ between 0.5 and 0.75 measured by IRAS (numbers SL 175–187). These objects are also YSO candidates (see Section 6). However, the identification of IRAS and 2MASS sources in some cases is problematic due to low accuracy of the IRAS coordinates.

In the Galactic coordinates (Figure 3) we plot 45 objects from Table 1 plus five objects from Paper II listed above. In the background, dust clouds from the Dobashi et al. (2005) atlas are shown. It is evident that the suspected YSOs concentrate in the densest clump of the DoH 942 cloud: 11 objects are crowded at ℓ, $b = 141.9–142.1°$, $+1.7 - +2.0°$, around the position of the high-mass YSO, GL 490. Hodapp (1990, 1994) described a smaller cluster at GL 490 seen on his K-band images. However (see the next section), clustering of infrared objects in the direction of a dense dust cloud is not necessary related to young objects.

3. DISTRIBUTION OF REDDENED K–M GIANTS IN THE AREA

With the aim to compare the surface distributions of the suspected YSOs and the reddened stars of normal spectral classes, we have separated 88 stars of the

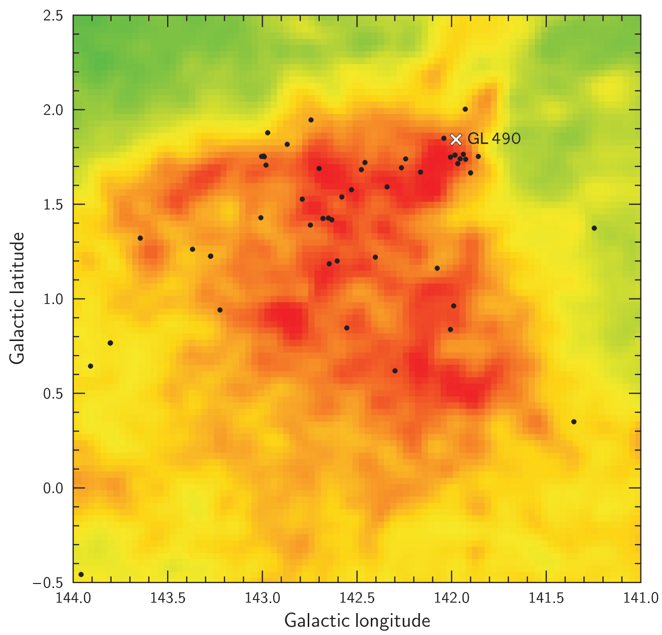

Fig. 3. Positions of the suspected YSOs in the GL 490 area in the Galactic coordinates. Dust clouds from the Dobashi et al. (2005) atlas are shown in the background. The position of the YSO GL 490 is shown by the white cross.

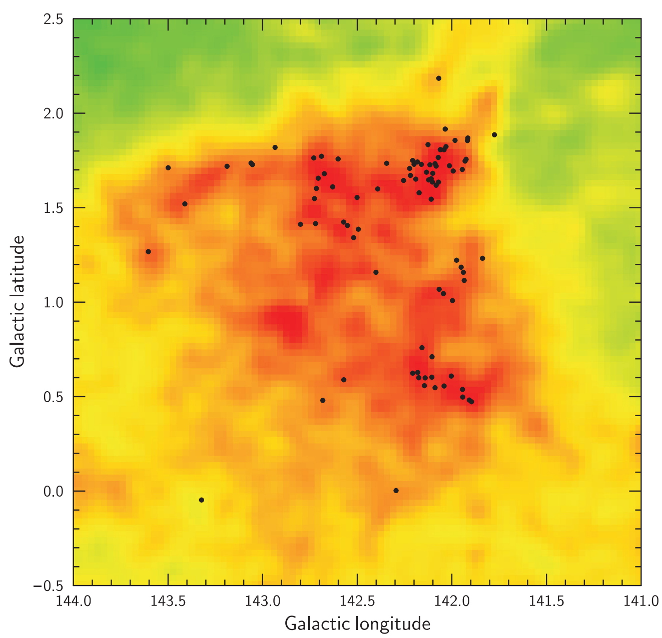

Fig. 4. Positions of the suspected K–M giants in the GL 490 area. Dust clouds are the same as in Figure 3.

upper 'tail' in Figure 2 satisfying the following conditions: (1) H–$K_s \geq 0.75$ and (2) $Q_{JHK} > 0.2$. These stars are listed in Table 3. In two-color diagram these stars are dispersed along the reddening line of K and M giants, therefore we use the letters K-M as the prefix to their numbers. Most probably they are field stars located behind the DoH 942 cloud, with the extinction A_V between 10 and 20 mag. K and M giants in the K passband are quite bright: absolute magnitudes M_K of K0 III and M5 III stars are –1.6 mag and –6.3 mag, respectively. Such stars appear in our sample even with heavy extinction and being located at distances of a few kpc. A simple calculation shows that at a distance of 1 kpc, where the DoH 942 cloud is supposed to lie, all main-sequence stars cooler than F5 V should be fainter than our limiting magnitude K = 12.5. Stars of spectral classes B and A should be also absent in the sample: they are excluded by condition (2) listed above, since their Q_{JHK} is close to zero.

We could not find any IRAS source among the selected 88 objects of the upper 'tail'. Only six sources were identified with MSX. This is an additional argument that these objects are normal K–M stars without dust envelopes. In the IRAS passbands they were too faint to be measured.

Table 3. Suspected heavily reddened K–M III stars with H–$K_s \geq 0.75$ in the $3° \times 3°$ area centered at ℓ, $b = 142.5°$, $+1.0°$.

K-M	ℓ	b	J	H	K_s	J–H	H–K_s	Q_{JHK}
01	141.775	1.886	14.77	12.93	12.11	1.84	0.82	0.32
02	141.838	1.232	13.00	10.28	9.03	2.72	1.25	0.40
03	141.896	0.473	15.12	13.22	12.37	1.89	0.86	0.31
04	141.908	0.482	14.32	12.63	11.88	1.68	0.75	0.29
05	141.916	1.869	12.33	10.45	9.64	1.88	0.81	0.39
06	141.918	1.855	13.80	12.12	11.35	1.68	0.76	0.27
07	141.925	1.756	13.98	11.85	10.84	2.14	1.01	0.26
08	141.930	1.747	13.00	10.76	9.71	2.23	1.05	0.28
09	141.935	1.115	12.23	10.27	9.44	1.96	0.83	0.42
10	141.939	1.158	14.34	12.46	11.66	1.88	0.80	0.41
11	141.943	0.498	13.96	12.07	11.24	1.89	0.83	0.36
12	141.944	0.538	13.52	11.84	11.08	1.68	0.76	0.27
13	141.945	1.702	14.22	12.46	11.69	1.76	0.78	0.32
14	141.951	1.185	14.49	12.59	11.80	1.91	0.78	0.46
15	141.975	1.222	10.56	8.78	8.03	1.78	0.76	0.38
16	141.983	1.856	11.00	9.09	8.20	1.90	0.89	0.26
17	141.993	1.694	14.65	12.80	11.98	1.84	0.82	0.33
18	141.997	1.008	15.31	13.44	12.64	1.86	0.80	0.38
19	142.003	0.609	15.46	13.83	13.07	1.63	0.76	0.22
20	142.013	1.722	15.41	13.28	12.29	2.12	1.00	0.28
21	142.031	1.823	13.91	11.03	9.66	2.88	1.37	0.34
22	142.035	1.916	15.11	13.34	12.58	1.74	0.79	0.29
23	142.041	1.807	13.87	12.02	11.18	1.85	0.84	0.31
24	142.041	0.556	14.91	12.88	11.98	2.02	0.91	0.34
25	142.045	1.045	14.56	12.88	12.12	1.69	0.75	0.29
26	142.061	1.807	14.10	12.22	11.38	1.88	0.83	0.34
27	142.067	1.068	12.04	10.11	9.31	1.93	0.79	0.46

Table 3. Continued

K-M	ℓ	b	J	H	K_s	J–H	H–K_s	Q_{JHK}
28	142.069	2.185	14.64	12.47	11.47	2.17	1.01	0.30
29	142.071	1.635	14.59	12.72	11.87	1.87	0.85	0.29
30	142.072	1.766	13.99	11.98	11.04	2.01	0.94	0.28
31	142.083	1.619	12.19	10.21	9.36	1.98	0.85	0.42
32	142.083	1.720	15.09	13.14	12.24	1.95	0.90	0.28
33	142.089	0.547	15.05	13.22	12.37	1.83	0.85	0.25
34	142.089	1.733	14.73	12.71	11.74	2.02	0.97	0.22
35	142.101	1.682	13.35	11.62	10.86	1.73	0.76	0.31
36	142.103	1.636	14.33	12.54	11.70	1.79	0.84	0.23
37	142.105	0.711	12.85	11.02	10.27	1.82	0.75	0.43
38	142.106	0.603	15.44	13.41	12.52	2.02	0.89	0.38
39	142.109	1.653	14.02	11.88	10.93	2.14	0.96	0.37
40	142.109	1.545	15.06	13.38	12.62	1.68	0.76	0.27
41	142.116	1.727	15.10	13.42	12.66	1.68	0.76	0.28
42	142.123	1.647	11.67	9.40	8.37	2.27	1.03	0.36
43	142.126	1.834	11.79	9.96	9.21	1.83	0.76	0.43
44	142.134	1.688	15.31	13.33	12.48	1.98	0.85	0.40
45	142.141	0.599	14.30	12.51	11.70	1.79	0.81	0.28
46	142.145	0.558	15.56	13.19	12.07	2.37	1.12	0.30
47	142.158	0.759	13.55	11.39	10.49	2.16	0.90	0.49
48	142.161	1.729	13.89	11.96	11.14	1.93	0.82	0.41
49	142.173	1.579	15.18	13.19	12.32	1.99	0.87	0.38
50	142.175	0.600	11.55	9.79	9.04	1.76	0.75	0.37
51	142.180	0.628	11.07	8.62	7.48	2.45	1.14	0.35
52	142.182	1.742	15.23	13.50	12.68	1.73	0.82	0.22
53	142.191	1.651	14.75	12.41	11.29	2.34	1.12	0.26
54	142.200	1.730	13.30	11.33	10.46	1.96	0.87	0.36
55	142.207	1.750	14.86	13.24	12.49	1.62	0.75	0.23
56	142.207	0.624	14.47	12.72	11.94	1.75	0.78	0.31
57	142.219	1.671	13.34	11.42	10.56	1.93	0.85	0.35
58	142.223	1.708	12.89	11.05	10.29	1.83	0.76	0.42
59	142.255	1.644	8.68	6.76	5.87	1.91	0.90	0.26
60	142.295	0.003	9.44	7.61	6.74	1.84	0.87	0.23
61	142.345	1.735	11.47	9.67	8.90	1.80	0.77	0.37
62	142.392	1.599	11.23	9.34	8.48	1.89	0.86	0.30
63	142.401	1.158	14.74	12.75	11.88	1.99	0.87	0.38
64	142.494	1.386	10.89	9.18	8.42	1.71	0.76	0.31
65	142.501	1.554	12.96	10.20	8.89	2.76	1.31	0.34
66	142.519	1.341	14.51	12.26	11.28	2.26	0.98	0.45
67	142.552	1.406	14.27	12.20	11.31	2.07	0.89	0.42
68	142.571	0.589	12.08	10.30	9.52	1.78	0.77	0.36
69	142.572	1.424	15.17	13.50	12.73	1.67	0.76	0.26
70	142.601	1.758	13.24	11.36	10.58	1.88	0.77	0.46
71	142.630	1.610	13.96	11.84	10.93	2.12	0.91	0.43
72	142.674	1.680	13.49	11.69	10.89	1.81	0.79	0.34
73	142.682	0.480	12.75	10.81	9.98	1.94	0.83	0.41
74	142.689	1.772	13.71	11.80	10.92	1.92	0.88	0.29

Table 3. Continued

K-M	ℓ	b	J	H	K_s	J–H	H–K_s	Q_{JHK}
75	142.706	1.656	12.47	10.70	9.94	1.77	0.76	0.37
76	142.716	1.602	11.51	9.65	8.82	1.87	0.83	0.33
77	142.720	1.416	14.57	12.67	11.86	1.90	0.81	0.41
78	142.726	1.548	12.18	10.36	9.60	1.83	0.76	0.43
79	142.730	1.763	14.20	12.33	11.51	1.86	0.82	0.35
80	142.800	1.412	14.74	12.97	12.21	1.77	0.76	0.37
81	142.934	1.819	9.48	7.75	6.96	1.74	0.79	0.27
82	143.054	1.728	13.48	11.22	10.17	2.26	1.05	0.32
83	143.061	1.736	12.97	11.00	10.09	1.97	0.91	0.29
84	143.188	1.719	9.84	8.09	7.30	1.75	0.79	0.29
85	143.323	–0.047	13.04	11.27	10.47	1.77	0.80	0.29
86	143.411	1.520	13.22	11.27	10.47	1.96	0.80	0.47
87	143.499	1.711	12.81	10.94	10.15	1.86	0.79	0.40
88	143.604	1.267	10.46	8.70	7.93	1.76	0.76	0.35

Figure 4 exhibits the surface distribution of the supposed heavily reddened K–M giants in the Galactic coordinates. One can find strong evidence that these stars have a tendency to concentrate in the direction of the densest dust clouds, showing similarity to the distribution of possible YSOs (Figure 3). However, K–M giants are distributed broader, they are not so concentrated to the GL 490 cloud as YSOs. We should expect that K–M giants in the background populate all the area with more or less uniform surface density, and many of them are present in the J–H vs. H-K_s diagram of Figure 2. However, their color indices H–K_s are < 0.75, consequently, they do not appear in Figure 4.

The tendency of both the YSOs and the heavily reddened K–M giants to concentrate apparently in the direction of dust clouds prevents using the clustering factor alone as approval of physical relation between the stars and the cloud. This can lead to misinterpretation of distant red giants as a cluster of infrared YSOs. However, this ambiguity can be avoided with *JHK* photometry at hand since K–M giants and YSOs are located in different 'tails' in the J–H vs. H–K_s diagram.

5. THE COMPARISON AREA

For a better understanding of the reliability of identification of YSOs and K–M giants we decided to apply the same procedure for an area located outside the dust cloud but close to the GL 490 area. We expect that such an area should contain almost the same amount of background K–M giants, AGB stars, galaxies and quasars which are the main YSO simulators. For this aim we selected the $3 \times 3°$ area centered at ℓ, $b = 144.0°$, $+3.5°$ which is shown in Figure 1.

The J–H vs. H–K_s diagram for 35 200 infrared objects, selected in the comparison area, is shown in Figure 5. Notice that the numbers of objects in both the GL 490 area and the comparison area are similar. However, their distribution in the two-color diagram is quite different. The upper 'tail' of K–M giants for the comparison area is quite short – the interstellar extinction A_V of the most reddened background stars does not exceed 4–5 mag. The lower 'tail', observed in the GL 490 area, is amost absent: we find only 10 stars near the intrinsic line of T Tauri stars and near the black-body line with H–$K_s > 0.75$. Six of them are IRAS

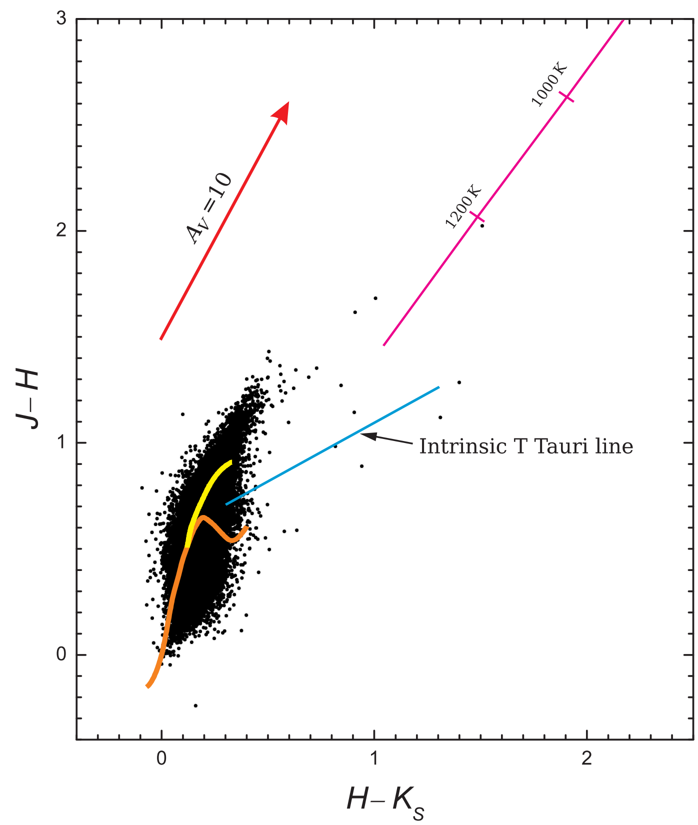

Fig. 5. The J–H vs. H–K_s diagram for 35 200 objects in the comparison area shown in Figure 1. The intrinsic main-sequence and K–M giant lines, the intrinsic locus of T Tauri stars, the locus of black bodies and the reddening vector are the same as in Figure 2.

and MSX objects, among them four objects are carbon stars and one object is a Mira variable (LL Cam).

6. SPECTRAL ENERGY DISTRIBUTIONS

The best way to discriminate between YSOs and old AGB objects (Mira variables, N-type carbon stars and OH/IR objects) is to construct infrared spectral energy distribution (SED) curves using the 2MASS, IRAS and MSX data. The 2MASS data alone are not sufficient since all these types of stars occupy the same area in the J–H vs. H–K_s diagram.

Table 2 of the present paper lists 25 objects in the vicinity of GL 490 which have reliable fluxes at least in one of the four IRAS passbands and/or have reliable MSX fluxes in the 8.3 μm passband. Their red F magnitudes at 710 nm were selected from the GSC 2.2 catalog. For all these objects SEDs were calculated as described in Paper II and for 12 of them are plotted in Figures 6 and 7. Almost all these objects exhibit strong infrared excesses at $\lambda > 2.2$ nm, i.e., probably they are pre-main-sequence objects in different evolutionary stages (Lada 1987; Robitaille

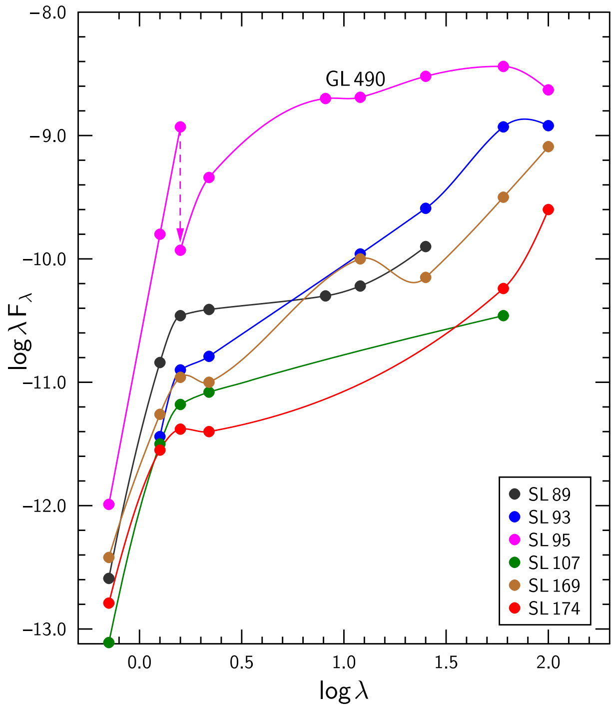

Fig. 6. Spectral energy distributions for six objects of Table 2 which are most similar to the Class I YSOs.

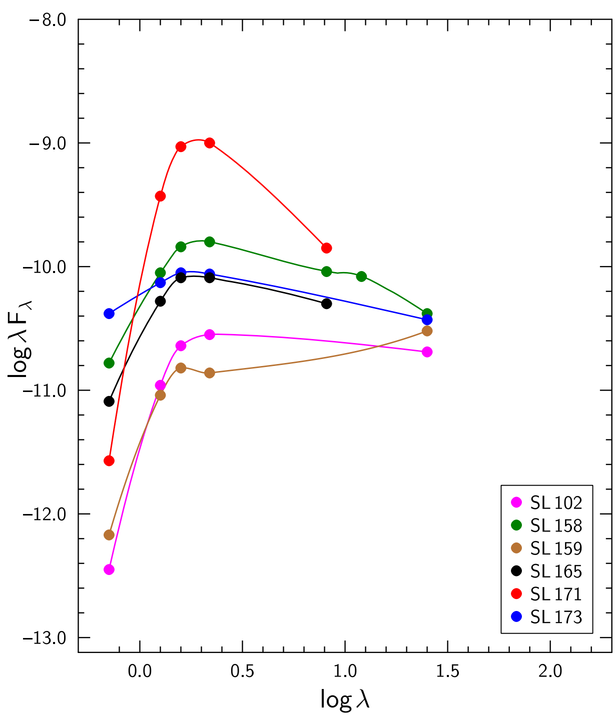

Fig. 7. Spectral energy distributions for six objects of Table 2 which are most similar to the Class II YSOs.

et al. 2006). Sixteen objects exhibit SEDs which are similar to Class I with a steep rise of the flux in the far infrared, eight are Class II objects with the flat flux, and one object (SL 171) may be a heavily reddened Herbig Ae/Be star or a distant AGB object.

Among the suspected K–M giants (upper 'tail'), only five objects were measured by MSX and no objects by IRAS (Table 4). SEDs of these stars are plotted in Figure 8. There is no doubt that all of them are similar to heavily reddened K–M stars without infrared excesses (compare this figure with Fig. 5 in Paper II). This confirms our claim that the upper 'tail' in the J–H vs. H–K_s diagram (Figure 1) is formed mainly by normal late-type giants.

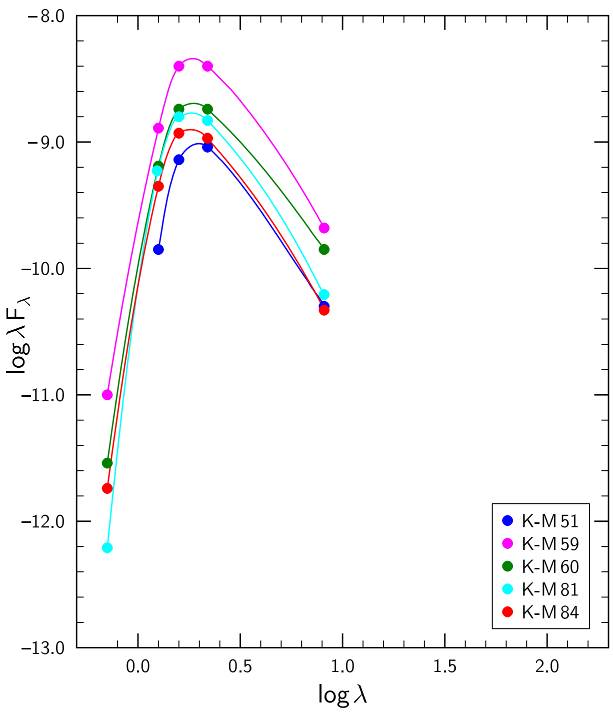

Fig. 8. Spectral energy distributions for five stars, suspected heavily reddened K–M giants.

Table 4. Stars of the GL 490 region located in the J–H vs. H–K_s diagram in the upper 'tail' and measured by MSX.

K-M	ℓ deg	b deg	RA (J2000) h m s	DEC (J2000) ° ′ ″	Flux at 8.3 μm Jy
51	142.180	0.628	03 23 45.33	+57 41 30.4	0.14
59	142.255	1.644	03 28 30.37	+58 29 37.6	0.58
60	142.295	0.003	03 21 56.11	+57 06 20.3	0.39
81	142.934	1.819	03 33 30.89	+58 15 00.7	0.15
84	143.188	1.719	03 34 38.41	+58 01 17.6	0.13

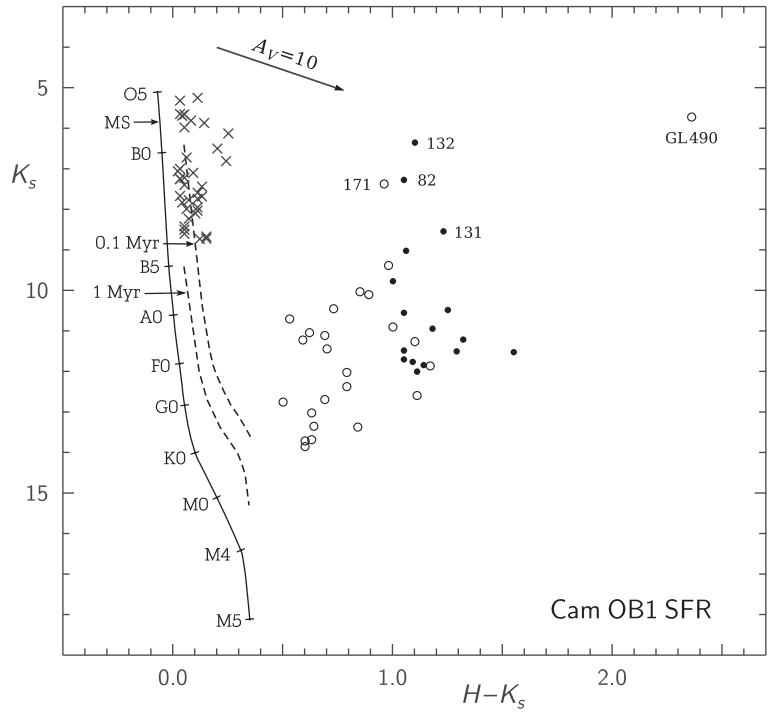

Fig. 9. The K_s vs. H–K_s diagram for the Cam OB1 star-forming region located at a distance of 900 pc. Open circles are YSOs from the GL 490 area of $3^\circ \times 3^\circ$ size, dots are YSOs from the Cam OB1 association area of $26^\circ \times 24^\circ$ size. Crosses are the Cam OB1 association stars of spectral classes O–B. The main-sequence and isochrones for 0.1 Myr and 1.0 Myr are also plotted.

7. NEAR INFRARED COLOR-MAGNITUDE DIAGRAM FOR THE CAM OB1 STAR-FORMING REGION

More information about YSOs can be obtained from the infrared color vs. magnitude diagrams. One of these, relating the K_s magnitude with the H–K_s color index, is presented in Figure 9 for YSOs belonging to the Cam OB1 SFR. Only the objects, whose dependence to YSOs has been confirmed by IRAS and/or MSX photometry, are plotted. Open circles designate 25 YSOs from the GL 490 $3 \times 3^\circ$ area (Table 2) and dots designate 16 YSOs belonging to the Cam OB1 SFR in the $26^\circ \times 24^\circ$ area from Paper II. The unreddened main sequence corresponds to a distance of 900 pc. The isochrones for the ages 0.1 and 1.0 Myr are from Hillenbrand & Carpenter (2000). In the color-magnitude diagram, along with the YSOs, we also plot O–B3 stars of the association (crosses). All of them are concentrated near the zero value of H–K_s. Some of B-stars are of luminosity classes IV and III, and they overlap the reddened O-type stars.

The distribution of YSOs in Figure 9 is the result of combined effects of variable masses, temperatures, ages, near infrared excesses (due to envelopes and disks) and extinctions (both interstellar and circumstellar). The additional scatter of objects is introduced by various orientations of envelope cavities for Stage I objects and rings for Stage II objects (see Robitaille et al. 2006, 2007). Sometimes,

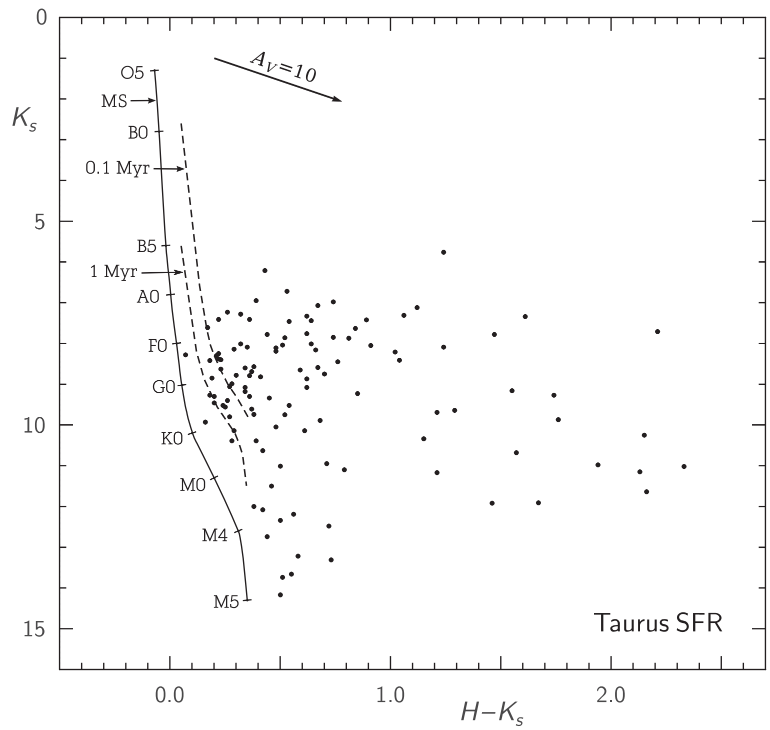

Fig. 10. The K_s vs. H–K_s diagram for YSOs of the Taurus star-forming region located at a distance of 150 pc. The data are from Briceño et al. (2002).

the magnitude of YSO is influenced by additional radiation of the surrounding reflection or emission nebula, consequently, the result depends on the aperture used. At the present stage of investigation we have no possibility to disentangle all these effects for individual objects.

The positions of YSOs in the K_s vs. H–K_s diagram above the main sequence can be explained by the following effects.

• The shift upward due to a larger diameter and luminosity: for a typical YSO age of 0.1 Myr the isochrone is above the main sequence by $\sim$3 mag.

• The shift upward and to the right due to near-infrared thermal emission in the circumstellar envelope or disk. According to Hillenbrand & Carpenter (2000) for the Taurus YSOs the K excess is from zero to $\sim$1.5 mag and the H–K excess is from zero to $\sim$0.8 mag, both excesses are linearly correlated.

• The shift down and to the right along the reddening lines due to extinction and reddening by the interstellar and circumstellar dust. The slope of the reddening line is $A_K/E_{H-K} = 1.79$ (Bessell & Brett 1988), and the ratio of extinctions is $A_K/A_V = 1.14$ (Cardelli et al. 1989). These ratios for the dust in the circumstellar envelope and disk can be somewhat different.

Probably, the best criterion for identifying YSOs of Stage I is their faintness in the visual wavelengths. In Figure 9 we find objects which are sufficiently bright in the J, H and K_s passbands but are invisible in the Palomar DSS2 red and blue

plates. These stars can be identified in Table 1 by the absence of magnitude in the F column. Such stars are also frequent in the Taurus clouds, despite their proximity to the Sun. Probably, this is caused by circumstellar dust shells and disks giving the extinctions A_V of the order of 30 mag and more (Myers et al. 1987; Whitney et al. 2003). However, if the object is directed to us by its envelope cavity or we are viewing along the disk axis, the circumstellar extinction is much smaller.

For comparison, the K vs. H–K_s diagram for YSOs in the Taurus SFR is presented in Figure 10, taking the K_s and H–K_s data from Briceño et al. (2002) and a distance of 150 pc. The $3 \times 3°$ area near GL 490 at a distance of 900 pc corresponds to $17 \times 17°$ at a distance of the Taurus SFR. This means that the real sizes of the GL 490 area and the Taurus SFR are more or less equal. Although the general appearance of the color-magnitude diagrams of the Cam OB1 and Taurus star-forming regions is similar, there are appreciable differences between them. We should not pay attention to the number differences of YSOs in both regions since the identification of YSOs in the Cam OB1 area (open circles in Figure 9) is affected by selection effects, such as the accuracy limit of 2MASS photometry, the presence or absence of the IRAS and MSX data, the limiting magnitude due to large distance, etc.

However, some differences are obvious. For example, the Cam OB1 SFR contains massive YSOs which are absent in the Taurus SFR. The most luminous in K_s is the object GL 490. Other objects brighter than $K_s = 9$ mag are SL 82, SL 131 and SL 132 from Paper II and SL 171 from Table 1 (numbered in Figure 9). The SED curves of these objects are of Class II, and there is a high probability that their masses correspond to A or B stars, i.e., they may belong to Herbig Ae/Be stars. Another alternative is that these stars are located in space closer to the Sun than we accepted.

Other difference between the two SFRs is in the number of objects with H–$K_s > 1.5$ – in Cam OB1 only GL 490 falls in this color range, while in Taurus such red objects are numerous, but at a lower luminosity level. No doubt, this effect originates in the accepted accuracy limit of H and K_s magnitudes (< 0.05 mag) in our study. This effect cuts off all the red objects fainter than $K_s = 14$ mag at H–$K_s = 0.6$ and fainter than $K_s = 12$ mag at H–$K_s = 1.5$.

8. J–H, H–K$_s$ DIAGRAM FOR THE CAM OB1 SFR

In Paper II the J–H vs. H–K_s diagram was given for real and suspected young objects belonging to the Local arm. Then only the YSOs with H–$K_s \geq 1.0$ were known. Now we have 20 additional suspected YSOs with H–K_s between 0.5 and 1.0. Thus, now we are able to plot a more complete two-color diagram for the objects in the Local arm. Since in the present paper we concentrate on the Cam OB1 star-forming region, we will ignore the YSOs from Paper II found to belong to the Gould Belt layer.

Figure 11 shows the J–H vs. H–K_s diagram for the same YSOs which were plotted in the color-magnitude diagram (Figure 9), but now all of them are shown as red dots. The dots between H–$K_s = 0.5$ and 1.0 designate objects of the $3 \times 3°$ area around GL 490, while the dots with H–$K_s \geq 1.0$ designate objects in the whole $26 \times 24°$ area. Additionally, we have plotted OB stars of the association Cam OB1 (black crosses), known irregular variables (blue dots) and the Hα emission stars (blue circles). Probably not all variables and emission-line stars belong to the Cam OB1 star-forming region, some may be located closer to the Sun. Figure 11 also

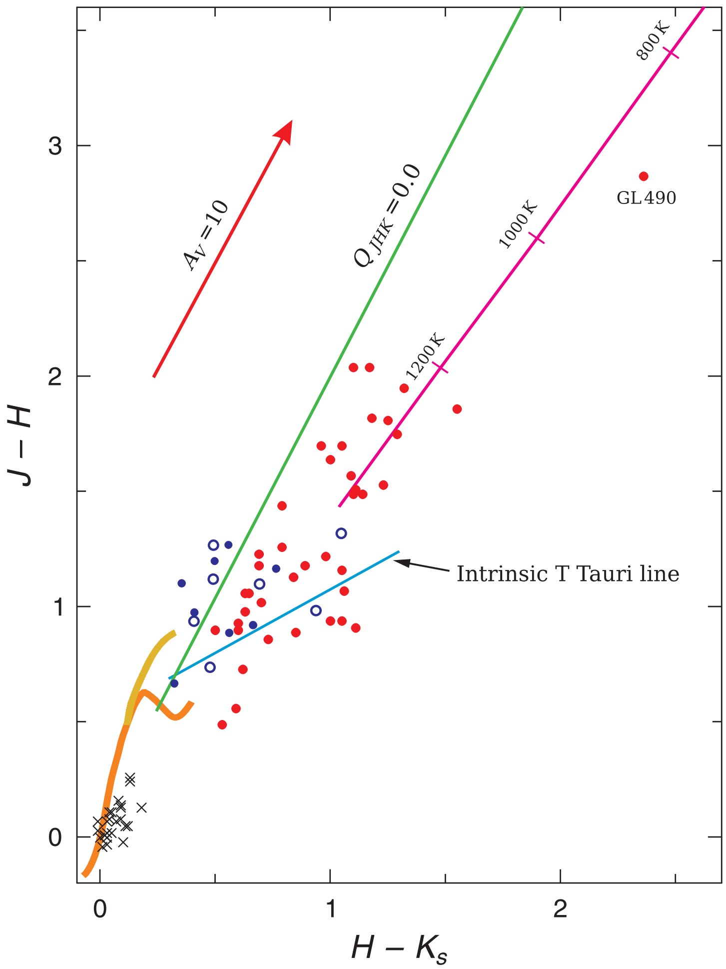

Fig. 11. The J–H vs. H–K_s diagram for the suspected YSOs (red dots) and other young objects in the Cam OB1 star-forming region. Black crosses are O–B3 stars of the Cam OB1 association, blue dots designate known irregular variables and blue open circles designate Hα emission stars. The intrinsic main-sequence and giant lines are shown in orange and yellow. The blue line designates the intrinsic locus of T Tauri stars (Meyer et al. 1997), the violet line is the locus of black bodies. The length of the reddening vector (in red) corresponds to the extinction in the V passband of 10 mag. Young stellar objects were searched for in the region below the green line.

shows the loci of normal luminosity V stars (orange curve) and red giants (yellow curve), the reddening vector for $A_V = 10$ mag (red), the reddening line of OB stars ($Q_{JHK} = 0.0$, green), the black-body line (violet) and the intrinsic line of T Tauri stars (blue).

It is evident, that the J–H vs. H–K_s diagram for YSOs in the Cam OB1 SFR is very similar to those in other SFRs. However, some red dots lie lower than the intrinsic line of T Tauri stars. Probably some of them (especially SL 175, SL 176 and SL 183) are heavily reddened Herbig Ae/Be stars or related objects in an

earlier evolutionary stage. These stars, like their counterparts above the intrinsic T Tauri line, exhibit infrared excesses at $> 2\ \mu$m.

9. CONCLUSIONS

In the dust cloud DoH 942, at the center of the Cam OB1 association, we have identified 50 infrared objects suspected to be in the pre-main-sequence stage of evolution. The criteria for the attribution of objects to YSOs were their positions in the J–H vs. H–K_s diagram and their spectral energy distribution curves constructed using the 2MASS, IRAS and MSX data. Among the 25 objects with the IRAS and/or MSX data we identify 16 YSOs of Class I, 8 YSOs of Class II and one object may be heavily reddened Ae/Be star or a background AGB star.

The MSX data confirm that the objects, forming the upper 'tail' in the J–H vs. H–K_s diagram, are background K–M giants heavily reddened by the DoH 942 dust cloud. The comparison field in the nearby area with a relatively low interstellar reddening does not contain objects which might be suspected as pre-main-sequence stars.

The suspected YSOs in the color-magnitude plane K_s vs. H–K_s occupy a large area located right of the main sequence, like YSOs in other star-forming regions (Orion, Taurus, etc.). This position can be explained by their luminosity, interstellar and circumstellar reddening and the infrared thermal emission from circumstellar envelopes and disks. However, the available data are not sufficient to disentangle all these effects for individual stars. However, some conclusions can be drawn for the most luminous objects like GL 490. The other three objects brighter than $K_s = 9$ mag (and some fainter objects) probably are heavily reddened Herbig Ae/Be stars or their prestellar counterparts.

ACKNOWLEDGMENTS. We are thankful to Bo Reipurth for useful comments and to Edmundas Meištas and Stanislava Bartašiūtė for their help preparing the paper. The use of the 2MASS, IRAS, MSX, SkyView and Simbad databases is acknowledged.

REFERENCES

Bessell M. S., Brett J. M. 1988, PASP, 100, 1134

Briceño C., Luhman K. L., Hartmann L., Stauffer J. R., Kirkpatrick J. D. 2002, ApJ, 580, 317

Cardelli J. A., Clayton G. C., Mathis J. S. 1989, ApJ, 345, 245

Cutri R. M., Skrutskie M. F., Van Dyk S., Beichman C. A. et al. 2003, *2MASS All Sky Catalog of Point Sources*, NASA/IPAC Infrared Science Archive, http://irsa.ipac.caltech.edu/applications/Gator/

Dobashi K., Uehara H., Kandori R., Sakurai T., Kaiden M., Umemoto T., Sato F. 2005, PASJ, 57, S1

Hillenbrand L. A., Carpenter J. M. 2000, ApJ, 540, 236

Hodapp K.-W. 1990, ApJ, 352, 184

Hodapp K.-W. 1994, ApJS, 94, 615

Lada C. J. 1987, in *Star Forming Regions* (IAU Symp. 115), eds. M. Peimbert & J. Jugaku, Reidel Publ. Comp., Dordrecht, p. 1

Meyer M. R., Calvert N., Hillenbrand L. A. 1997, AJ, 114, 288

Myers P. C., Fuller G. A., Mathieu R. D., Beichman C. A., Benson P. J., Schild R. E., Emerson J. P. 1987, ApJ, 319, 340

Robitaille T. P., Whitney B. A., Indebetouw R., Wood K., Denzmore P. 2006, ApJS, 167, 256

Robitaille T. P., Whitney B. A., Indebetouw R., Wood K. 2007, ApJS, 169, 328

Skrutskie M. F., Cutri R. M., Stiening R., Weinberg M. D. et al. 2006, AJ, 131, 1163

Straižys V., Laugalys V. 2007a, Baltic Astronomy, 16, 167 (Paper I)

Straižys V., Laugalys V. 2007b, Baltic Astronomy, 16, 327 (Paper II)

Whitney B. A., Wood K., Bjorkman J. E., Wolff M. J.. 2003, ApJ, 591, 1049